Electrorheological fluids with high shear stress based on wrinkly tin titanyl oxalate

ACS APPLIED MATERIALS & INTERFACES

Article

The Electrorheological Fluids with High Shear Stress Based on Wrinkly Tin Titanyl Oxalate

Jinghua Wu, Lei Zhang, Xing Xin, Yang Zhang, Hui Wang, Aihua Sun, Yuchuan Cheng, Xinde Chen, and Gaojie Xu

ACS Appl. Mater. Interfaces, **Just Accepted Manuscript** • DOI: 10.1021/acsami.8b00869 • Publication Date (Web): 01 Feb 2018

ACS Publications

ACS Applied Materials & Interfaces is published by the American Chemical Society. 1155 Sixteenth Street N.W., Washington, DC 20036

The Electrorheological Fluids with High Shear Stress Based on Wrinkly Tin Titanyl Oxalate

Jinghua Wu,[†,#] *Lei Zhang,*[†,‡,#] *Xing Xin,*[§] *Yang Zhang,*[⊥] *Hui Wang,*[†] *Aihua Sun,*[†] *Yuchuan Cheng,*[*,†] *Xinde Chen,*[//] *Gaojie Xu*[†]

[†]Zhejiang Key laboratory of Additive Manufacturing Materials, Ningbo Institute of Materials Technology & Engineering, Chinese Academy of Sciences, Ningbo, 315201, P. R. China

[‡]Nano Science and Technology Institute, University of Science and Technology of China, Suzhou 215123, China

[§]GREEN, National Institute for Materials Science, 1-1 Namiki, Tsukuba 305-0044, Japan

[⊥] Electron Microscopy for Materials Science (EMAT), University of Antwerp, Groenenborgerlaan 171, 2020 Antwerp, Belgium

[//] Guangzhou Institute of Energy Conversion, Chinese Academy of Sciences, Guangzhou, 510640, P. R. China

KEYWORDS: smart fluid, electrorheological, wettability, shear stress

ABSTRACT.

Electrorheological (ER) fluids are denoted as a type of smart fluids because their rheological characteristics can be altered through an electric field. The discovery of giant ER effect revived the researchers' interest in the ER technological area. However, the poor stability including the insufficient dynamic shear stress, large leakage current density as well as the sedimentation tendency still hinder its practical applications. Herein, we report a facile and scalable co-precipitation method for synthesizing surfactant-free tin titanyl oxalate (TTO) particles with tremella-like wrinkly microstructure (W-TTO). The W-TTO based ER fluids exhibit enhanced ER activity compared with the pristine TTO due the improved wettability between the W-TTO and silicone oil. In addition, the static yield stress and leakage current of the W-TTO ER fluids also show fine time stability during the 30 days tests. More importantly, the dynamic shear stress of W-TTO ER fluids can maintain stable among the whole shear rate range, which is valuable for their use in the engineering applications. The results in this work provided a promising strategy to solve the long-standing problem of ER fluid stability. Moreover, this convenient synthesis route may be considered a green approach for mass production of giant ER materials.

INTRODUCTION

Smart materials are a type of designed materials that can modulate their properties in a controlled fashion by external stimuli, such as changes of temperature, pressure, moisture, pH or electro/magnetic fields. As one of the most important field-responsive smart materials, electrorheological (ER) fluid has drawn plenty of attentions from academia, industry and government due to their unique rheological characteristics.[1,2] ER fluids are consist of the dielectric micro/nano-particles and the insulating oil, which exist as liquids in normal conditions. After applying external electric field, these materials transform quickly from liquid state to nearly solid state, and exhibit an order of magnitude increase of stress and shear modulus.[3-9] The characteristic provides an efficient way in the active and semi-active control devices, such as clutches, artificial skins and robotics.[10-15] As a result, ER fluids have a large available potential in the future market. However, ER fluids have long suffered from their limited mechanical performance (including static yield stress and shear stress) over the past several decades.[16-23]

In 2003, Wen et al discovered a novel ER fluid based barium titanyl oxalate (BTO) nanoparticles whose static yield stress was one order of magnitude higher than that of the previous ER fluids.[24] In order to distinguish with the traditional ER fluids, this high static yield stress ER fluid is called giant ER (GER) fluid. The emergence of giant rheological fluid set off a new round climax of research. The researcher observed the static yield stress of GER fluids is linearly dependence on the electric field, rather than an exponential relationship. It means the mechanism in the GER fluid is significantly different from the dielectric mechanism. Many phenomenological model, such as the saturation surface polarization, saturated orientation polarization and polar molecule dominated theory were proposed to explain the giant ER effect.

Although details are different, the polarization of molecular dipoles in the nanogap between two adjacent particles are considered as playing the decisive role in GER effect.[25-27] In terms of materials synthesis, several ER materials that possess GER effect were fabricated except the barium titanyl oxalate, such as Fe_2O_3 nanofluids prepared in ethylene glycol (EG), 1D calcium and titanium precipitate and a mesoporous cerium-doped TiO_2.[28-30]

Recently, the development of ER fluid with high and stable dynamic shear stress has been proposed to meet the rapid growth demand for practical applications. The dynamic shear stress has more important meaning than the static yield stress in most practical applications, because it means the ER fluids could work stably in the whole range of the shear rate, while the static yield stress is the maximum point in the stress-strain or stress-rate relation. Despite GER fluids show good static rheological properties, their dynamic shear stress has remained relatively limited. The shear stress become unstable once the strain or shear rate beyond the yield point. It is a universal disadvantage of GER fluids. Hence, designing a tunable GER fluids with high and stable dynamic shear stress is still an arduous challenge.

In this paper, we report a facile and scalable co-precipitation method for synthesizing tin titanyl oxalate (TTO) with tremella-like wrinkly microstructure. These polarizable particles with unique morphology yield promising results for solving the dynamic shear stress problems.[31-35] ER fluids based on these 3D wrinkle-type tin titanyl oxalate (W-TTO) particles exhibited both enhanced static yield stress and stable dynamic shear stress. The excellent ER rheological performance structure for the W-TTO ER fluids offers a way to develop novel particles for ER fluid applications. Moreover, the present route even can be scaled up as a green chemistry method for the industrial manufacture. Based on the morphology and dielectric analysis, we infer that the exceptional ER activity and stable dynamic rheological performance is in large part due

the unique structure and fine wettability between the W-TTO particles and insulting silicone oil. This work provides a new strategy for the future development of high activity ER fluids and hence promote their practical application.

EXPERIMENTAL SECTION

Chemicals: Tetrabutyl titanate (TBT, 98%), tin chloride ($SnCl_2 \cdot 2H_2O$, A. R.), sodium dodecylbenzenesulfonate (SDBS, A. R.) and oxalic acid ($H_2C_2O_4 \cdot 2H_2O$, A. R.) were purchased from the Sinopharm Chemical Reagent Company (Shanghai, China). All of the chemicals cited above were used as received without further purification. Deionized (DI) water from a Millipore-Q purification system (Milli-pore, USA) with a resistivity of 18.2 MΩ cm was used in this work.

Synthesis: The TTO particles were synthesized via a precipitation process. In a typical procedure, 11.28 g $SnCl_2 \cdot H_2O$and 17 ml titanium butoxide (TBT) were dissolved in 200 ml ethanol to form a transparent uniform suspension A. 12.6 g oxalic acid was dissolved 200 ml water/ethanol solution (1:1, in volume) to form a suspension B. After stirring for 1h, solution A was dropwise added into solution B. The resulting opalescent precipitate was further stirred for 4h. After aging for 6 h, the precipitate was collected by vacuum filtration, washed with copious amounts of water and ethanol in turns, and finally dried at 80 °C for 12h and 120 °C for another 4 h. The W-TTO was synthesized using the same synthesis procedures, while 5g SDBS was added in the solution B before the oxalic acid.

Preparation of the ER fluids: All the silicone oils (η = 10 mPa·s, dielectric constant = 2.5, density = 0.94 g cm^{-3}, 25°C) were dried at 120 °C for 2 h before the experiments. An ER suspension was prepared by dispersing the particles in silicone oil via grinding. The density of

the samples are measured by drainage method using a 5 mL pycnometer, and the density of the TTO and W-TTO are 4.3 and 4.2 g cm^{-3}, respectively.

Characterization: Powder X-ray diffraction (XRD) patterns were collected by a Bruker D8 Advance/Discover diffractometer with Cu Kα radiation. The morphology and HAADF-STEM mapping of the samples were examined using a Hitachi S4800 field emission scanning election microscope (FESEM) and an FEI Tecnai G2 F20 transmission-electron microscopy (TEM). The FTIR spectra were recorded using a Nicolet 6700 IR spectrometer. The element contents of the TTO and W-TTO samples were determined by inductively coupled plasma (ICP) atomic emission spectroscopy (Seiko SPS1700HVR). X-ray photoelectron spectroscopy (XPS) data were recorded using the AXIS Ultra DLD system (Kratos). The Brunauer–Emmett–Teller (BET) surface area by N_2 sorption were measured by a Micromeritics ASAP 2020 surface area and porosity analyzer.

The rheological properties were measured using a circular rheometer (Haake RS6000). The static yield stress was obtained by the stress-strain model at a very low shear rate (0.1 s^{-1}), the stress value at the abrupt decrease point of the viscosity was defined as the static yield stress. The flow curves for the shear stress vs shear rate were measured using the controlled shear rate (CR) mode for the shear rate range from 0.1 to 100 s^{-1}. All of the measurements were performed at room temperature.

RESULTS AND DISCUSSION

The morphology of the TTO and W-TTO particles were examined by SEM and TEM. Without the addition of SDBS, the TTO sample showed ball particles with smooth surface (Figure 1a and b). After adding the surfactant, the morphology of particles changes obviously (Figure 1c and d), the ball-like particles are replaced by the tremella-like particles. The TEM images reveal that the entire "tremella" is composed of intercrossed wrinkles, the wrinkles connected with each other to form a 3D porous architecture. The BET surface area of these samples is obtained bay N_2 adsorption-desorption measurement. Compared with TTO particles (24.6 m^2 g^{-1}), the BET surface area for W-TTO particles (120.8 m^2 g^{-1}) increases by nearly 5 times (Figure S1, S2), which means the 3D wrinkly microstructure can provide a large active interface in the electric filed. SDBS as a surfactant can change the interface properties between the titanium butoxide and water, and then results in the changes of particle size and shape. The SDBS in this reaction is considered to relevant to the stereochemistry and charge.[36] Generally, as an anioic surfactant, the SDBS molecule can be ionized into DBS-, then these charged ions can be adsorbed on the particle surface selectively, facilitating the formation of sheet-like structure.

The elemental mapping images of TTO and W-TTO particles are shown in Figure 1e and S3. From these mapping images, it can be observed that the Sn, Ti, C and O elements are filled in the whole TTO particles. Meanwhile, the Sn element is obvious thinner than the Ti element at the edge of W-TTO particles, indicating the content of Sn element is relatively lower compared with the content of Ti element in this area. To further illustrate this appearance, XPS and ICP test had been done. The ICP and XPS results show that the ratio of Sn and Ti element contents in TTO is 1.17:1 and 1.07:1, respectively; and for W-TTO, its ratio is 1.21:1 and 0.27:1 (Table S1). From the ICP result for W-TTO compared to that of TTO, Sn to Ti decreased 7.06% and 10.76%, respectively. The XPS data generally reflect the element information of the sample surface

within 10 nm, whereas the ICP data represent the overall composition of the sample. Hence, the above results quantitatively illustrate the distributions of Sn and Ti elements in the surface are different from those in the internal of the W-TTO particles. In addition, no obvious S 2p peak is observed in the XPS spectra of W-TTO particles (Figure S4, S5), indicating the SDBS added at the time of preparation has been washed clearly.

FTIR spectra were also measured to verify the formation of TTO and W-TTO particles (Figure 1f). The broad band at approximately 3430 cm^{-1} is attributed to the stretching vibration of –OH group. The band at 1680 and 1610 cm^{-1} are assigned to the vibration of carbonyl from the oxalates or related to O-H in absorbed water in $TiOC_2O_4(H_2O)_2$. The peaks at 1402 and 1343 cm^{-1} are attributed to the metal-carboxylate ($M\text{-}COO^-$) symmetric stretching. In addition, the shoulder peaks at 910 cm^{-1} is consistent to the Ti=O bond,[37] which should attribute the intercrossed wrinkle-like fringe and indicate the Ti exist as amorphous state in the particles. The band at 790 cm^{-1} are due to the C-C vibration mode. The band at 531 cm^{-1} is assigned to C-O in-plane bending. The peaks between 400 and 500 cm^{-1} are attribute to the Ti–O stretching vibration. It is noteworthy that no obvious benzene rings and alkane bands are observed in Figure 1f, which implies the SDBS ions may have been washed out of the W-TTO particles. The corresponding XRD patterns of the TTO and W-TTO are shown in Figure 1g, which are match well with the tin oxalate (SnC_2O_4) (JCPDS NO. 51-0614). The unidentified peaks can be attributed to $TiOC_2O_4(H_2O)_2$ and $TiO(OH)_2$, since it is difficult to obtain crystalline $TiOC_2O_4(H_2O)_2$ and $TiO(OH)_2$ precipitates. Combined with the results of ICP, XPS and IR, it can be deduced that the TTO particles are composed of SnC_2O_4, $TiOC_2O_4(H_2O)_2$ and $TiO(OH)_2$ compounds. The component of the W-TTO particles is similar to the TTO particles, the key different is that the main ingredient in the surface layer of the W-TTO is $TiOC_2O_4(H_2O)_2$ and

$TiO(OH)_2$. According to our previous work, the amorphous carboxyl groups from $TiOC_2O_4(H_2O)_2$ can form the polar interaction with the silicone oil, then reduce the interface energy.[37,38] Consequently, we deduce that the W-TTO particles have a better wettability compare to the TTO particles.

The wettability of dielectric materials has an impact effect in the particles dispersion in the insulting oil, which is one of main factors that determine the ER activity of the ER fluids. The dielectric particles with inferior wettability tend to aggregate into clusters driven by their lyophobic attractive force, which would result in a weak interparticle interaction than those well-dispersed particles. To evaluate the wettability of the TTO and W-TTO particles, the permeability of TTO and W-TTO particles were compared by the Washburn method.[39] The corresponding result is shown in Figure S6, it can be found that the wettability of the W-TTO particles was enhanced obviously compared with the TTO particles, which is in good agreement with our prediction. Our previous study indicated that the good wetting performance can reduce the field-off viscosity effectively.[38,40] Hence, we also compared the viscosity of two fluids (the volume fractions are 19%) in the absence of external electric field. As shown in Figure S7, the two suspensions represent approximate newton behavior at the same volume fraction, their shear stresses show direct proportion to the shear rates, and the apparent viscosities are 6 and 4.5 Pa·s, respectively. The above result further verified that the presence of the $TiOC_2O_4(H_2O)_2$ ultrathin layer improved the wettability hence lead to low field-off viscosity.

The electric field response of TTO and W-TTO ERF (the volume fractions are 19%) had been observed through an optical microscope (Figure 2). Without the electric field, the TTO and W-TTO particles in the ER fluids dispersed randomly in the insulating oil. After an external electric field was applied, both TTO and W-TTO particles oriented along the direction of electric field

(Figure 2b, e). However, there still exists some differences between their moving processes. After the electric filed is applied, the W-TTO particles move more rapidly than the TTO particles. Furthermore, the chains formed by the W-TTO particles are denser and thicker than that of the TTO particles (Figure 2c and f, dashed line box is the enlarged view). These phenomena indicate that the ER performance of the W-TTO is superior to that based on the TTO particles.

The static yield stresses of the TTO and W-TTO suspensions were evaluated under different electric field. As shown in Figure 3, both TTO and W-TTO ER fluids, their static yield stresses show the near-linear dependence behavior when the electric field strength exceed a critical number $Ec \approx 1$ kV mm^{-1}. The static yield stresses of the TTO ER supspersons are 19 kPa, 36 kPa and 64 kPa (4 kV mm^{-1}), when the volume fractions are 19%, 32% and 41%, respectively. In contrast, the W-TTO ER fluids show obviously higher ER activity with static yield stresses as high as 23 kPa, 47 kPa and 88 kPa, which were promoted significantly than the TTO ER fluids. In principle, the linear dependency of the static yield stress is a direct reflection of the surface saturation polarization.[7] Generally, the static yield stress is positive correlation with the electric energy density PE, where E is the local electric field. P is polarizability, which is presumed to be a constant in the saturation polarization and independent of E. The results of static yield stress analysis indicate that the polarizability of the W-TTO particles is larger than the TTO particles. More than that, the static yield stresses are evaluated under different temperature. It can be seen in Figure 3c and d, two ER fluids exhibit a stable reliable stability under the whole temperature range from -20 ^{o}C to 100 ^{o}C, only show a little increase at 40 ^{o}C. The relative standard deviations of the static yield stress (4 kV mm^{-1}) of the TTO ER fluid and W-TTO ER fluid at different temperature are only 6.8% and 5.4%, respectively. It implies these two kinds of ER fluids

possess wide operate temperature range, which is very meaningful for practical application. The leakage current density is an important criterion to evaluate the use safety of the ER fluids. Figure 3e and f shows the leakage current density of the TTO and W-TTO ER fluids. The maximum current density of W-TTO ER fluid is less than 6.5 μA cm^{-2}, indicating the W-TTO materials possess high operation safety and low power consumption. In addition, the current densities are obviously lower than that of the TTO ER fluid. The reduced current density should attribute to the well wettability of the W-TTO particles. The insulating silicone oil thin layer between the neighbouring particles would restrain the charges migration under the electric field (Figure 3g, h), and result in low leakage current density.[41]

Dynamic rheological properties of TTO and W-TTO ER fluids (only 32% and 19%, the shear stress of 41% W-TTO ER fluid is beyond the measuring range of our rheometer) are shown in Figure 4 and S8-S11. When there is no electric field applied, the ER fluids show a light departure from Newtonian fluid (Figure S7). When an electric field is present, the shear stress increase greatly and act as plastic fluids, which are attributed to the chain-like structure formed under external electric field. The shear stress of the W-TTO ER fluid are obviously higher than that of the TTO under the same electric field strength and volume fraction. Dynamic rheological behavior is mainly dominated by the synergy between the electrostatic interaction induced by the electric field and the hydrodynamic forces caused by the shear field. The electrostatic interaction are responsible for the maintenance of the ER chain structure and hinders the flow, while the hydrodynamic interaction forces tends to destroy chain structure and motivates flow. Hence the high and stable shear stress of W-TTO ER fluids further confirms the W-TTO particles possess not only large polarizability but also fast response time to keep the structures and rheological properties stable.[42-45] Compared the flow curves of TTO ER fluids with those of W-TTO ER

fluids (Figure S8, S10 and Figure 4a, c), it is observed that the shear stresses of both low concentration (19%) ER fluids remain stable during the entire shear rate range under different electric field strength. When the concentration increases to 32%, the shear stress of the W-TTO ER fluids still maintains a stable level; but for the TTO ER fluids, the shear stress reaches a maximum value, then decreases rapidly. The main reason for the quick decrease of shear stress in the high concentration TTO ER fluids is the phase separation between the dielectric particles and the silicone oil. Under high shear rate, the column-like structures assembled by TTO particles migrate to the outer edge of the electrode due to the centrifugal force from the rotating motion, resulting in a decrease in the solid content between the electrode plates.[46] The thicker the ER fluids is, the more obvious the phenomenon becomes. However, this phenomenon is avoided effectively for the W-TTO ER fluids, because the W-TTO particles possess fine wettability with the silicone oil. In the W-TTO ER fluids, the silicone oil can spread out over the surface of W-TTO particles sufficiently, the oxygen atoms of silicone oil molecular chains and the carboxylic acid group on the W-TTO particle surfaces form hydrogen bonding network. Moreover, the polar groups of the W-TTO particles form the aligned dipolar filaments which bridge the two particles' confinement boundaries and finally penetrate the silicone oil film.[47] These forces help the silicone oils to catch the W-TTO particles tightly, avoids them migrated to the outer edge of the electrode acting by the outward centrifugal force. As a result, the measured shear stress of high concentration W-TTO ER fluids keeps stable under shear flow.

According to the polarization theory, the ER materials are polarized due to the dielectric mismatch between the insulating liquid and ER materials.[48] High polarizability and fast response time of ER particles are very vital to induce strong ER activity and stable ER rheological performance under shear flow. It is well-known that the polarization theory describes

polarization of the ER fluids using the complex dielectric constant ε=ε'-iε", where the real part ε' and the imaginary part ε" are the dielectric constant and dielectric loss factor, respectively. According to the mechanism proposed by Block et al, large Δε' and the suitable location of ε" in the range of 10^2 to 10^5 Hz would generate strong ER activity and maintain the stable chain structure of the ER particles.[49] The ε" peak is related to the proper response velocity, characterized by the relaxation time $\tau=1/2\pi f_{max}$, where the f_{max} is frequency of the ε" peak.[50,51] The dielectric spectra of the TTO and W-TTO ER fluids is shown in Figure S12, and many dielectric characteristics were calculated in table 1. The Δε' of the W-TTO suspension (18.84) is obvious larger than that of the TTO suspension (8.73), implying it could induce larger polarizability, which is responsible for its improved ER activity. Furthermore, the W-TTO ER suspension shows a dielectric relaxation peak at higher frequency location, meaning shorter response time. The larger Δε' and shorter response time of the W-TTO ER fluid induce a stronger and stable flow performance.

Time stability is also a decisive character to verify whether one ER material can be adopted for future practical application. In order to comprehensively evaluate the TTO and W-TTO ER fluids, their gravitational settling properties were recorded. Figure 5a presents the sedimentation stability of TTO and W-TTO ER fluids. It can be observed that the sedimentation lead to obvious phase separation in TTO ER fluids, the sedimentation ratio of TTO ERF is only 82.7% after 30 days. Meanwhile, the sedimentation ratio of W-TTO ERF reaches 91.1%. Considering that the density of the two samples are similar, the improved anti-settleability of the W-TTO particles should be attributed to the better wettability with silicone oil and the porous structure. Well anti-settle ability are helpful to obtain fine stress stability for long time operation, especially for the practical application, because the ER activity would decrease greatly along with the phase

separation of the ER suspensions. To evaluate the effect of sedimentation on the ER performances, the static yield stress and leakage current density of the TTO and W-TTO ER fluids are inspected after standing for 30 days (Figure S13-S16). Figure 5b and c plotted the difference in the static yield stress and leakage current density between before and after standing, respectively. The two types of ER fluids display different performances in time stability. The static yield stresses of TTO fluids decrease obviously as time goes on. Meanwhile, the leakage current density increases dramatically, jumps by as much as 127%. It should be ascribed the agglomeration of TTO particles caused by the phase separation, which would accelerate the charge migration under external electric field. Compared with the TTO ER fluid, the change of the W-TTO ER fluid is small, indicating the time stability superiority of the W-TTO materials is remarkable.

What's more, the convenient method can be considered as a practical route and can be enlarged for future industrial manufacture. A batch of 200 g products (Figure 6a and b) has been successfully obtained using a ten liter reaction unit (experiment conditions kept unchanged except the volumes of the reactants were scaled up), which show the high controllability. The results of SEM and XRD show the products have similar morphology and composition to that acquired by small reaction (Figure 6c and d). More importantly, the relevant activity of the W-TTO ER fluid prepared at a large scale (Figure 6e) show an excellent performance about the stress and leakage current under various electric fields (the volume fraction of ER fluid of large-scale sample is 41%).

CONCLUSION

In summary, we had successfully prepared a tremella-like W-TTO particles with 3D wrinkle microstructure via a facile precipitation route. The 3D microstructure provides high specific surface area and fine wettability with the silicone oil, resulting in large active interface in the applied electric filed. Consequently, the ER fluid composed of the W-TTO particles exhibits excellent rheological properties, time stability and temperature stability. More importantly, the W-TTO ER fluids exhibit excellent dynamic shear stress stability among the whole shear rate range, which is valuable for its using in the electric–mechanical interfaces. The excellent comprehensive performance prompts the W-TTO ER fluids to be a very promising candidate with real practical value. Furthermore, our work also provides a useful strategy to obtain enhanced ER activity and improved stability for ER material design by optimizing its wettability.

ASSOCIATED CONTENT

Supporting Information.

The Supporting Information is available free of charge on the ACS Publications website at DOI:

Nitrogen isotherm adsorption–desorption curves of TTO and W-TTO, elemental mapping images of TTO, XPS spectra of TTO and W-TTO, dielectric spectra of TTO and W-TTO suspensions, flow properties and leakage current density of TTO and W-TTO ER fluids with/without electric field.

AUTHOR INFORMATION

Corresponding Author

*E-mail: yccheng@nimte.ac.cn

Author Contributions

#J. Wu and L. Zhang contributed equally to this work.

Notes

The authors declare no competing financial interest.

ACKNOWLEDGMENT

The work was supported by the National Natural Science Foundation of China (Grant 21573267, 11674335), the Youth Innovation Promotion Association CAS (2013196), the Program for Ningbo Municipal Science and Technology Innovative Research Team (2015B11002, 2016B10005).

REFERENCES

(1) Sheng, P.; Wen, W. Electrorheological Fluids: Mechanisms, Dynamics, and Microfluidics Applications. *Annu. Rev. Fluid Mech.* **2012**, 44, 143-174.

(2) Hao, T. Electrorheological Fluids. *Adv. Mater.* **2001**, 13, 1847-1857.

(3) Yin, J.; Zhao, X.; Xiang, L.; Xia, X.; Zhang, Z. Enhanced electrorheology of suspensions containing sea-urchin-like hierarchical Cr-doped titania particles. *Soft Matter* **2009**, 5, 4687-4697.

(4) Choi, H. J.; Jhon, M. S. Electrorheology of Polymers and Nanocomposites. *Soft Matter* **2009**, 5, 1562–1567.

(5) Lee, S.; Lee, J.; Hwang, S. H.; Yun, J.; Jang, J. Enhanced Electroresponsive Performance of Double-Shell SiO_2/TiO_2 Hollow Nanoparticles. *ACS Nano* **2015**, 9, 4939–4949.

(6) McIntyre, C.; Yang, H.; Green, P. F. Electrorheology of Suspensions Containing Interfacially Active Constituents. *ACS Appl. Mater. Interfaces* **2013**, 5, 8925-8931.

(7) Shen, R.; Wang, X. Z.; Lu, Y.; Wen, W. J.; Sun, G.; Lu, K. Q. The methods for measuring shear stress of polar molecule dominated electrorheological fluids. *J. Appl. Phys.* **2007**, 102, 024106.

(8) Tan, P.; Huang, J.; Liu, D.; Tian, W.; Zhou, L. Colloidal electrostatic interactions between TiO_2 particles modified by thin salt solution layers. *Soft Matter* **2010**, 6, 4800-4806.

(9) Liu, Y. D.; Choi, H. J. Electrorheological fluids: smart soft matter and characteristics. *Soft Matter* **2012**, 8, 11961-11978.

(10) Lee, S.; Kim, Y. K.; Hong, J. Y.; Jang, J. Electro-response of MoS_2 Nanosheets-Based Smart Fluid with Tailorable Electrical Conductivity. *ACS Appl. Mater. Interfaces* **2016**, 8, 24221-24229.

(11) Shin, K. Y.; Lee, S.; Hong, S.; Jang, J. Graphene Size Control via a Mechanochemical Method and Electroresponsive Properties. *ACS Appl. Mater. Interfaces* **2014**, 6, 5531-5537.

(12) Yin, J.; Zhao, X.; Xia, X.; Xiang, L.; Qiao, Y. Electrorheological fluids based on nano fibrous polyaniline. *Polymer* **2008**, 49, 4413-4419.

(13) Yin, J.; Xia, X.; Xiang, L.; Zhao, X. Coaxial cable-like polyaniline@titania nanofibers: facile synthesis and low power electrorheological fluid application. *J. Mater. Chem.* **2010**, 20, 7096–7099.

(14) Yin, J.; Wang, X.; Chang, R.; Zhao, X. Polyaniline decorated graphene sheet suspension with enhanced electrorheology. *Soft Matter* **2012**, 8, 294–297.

(15) Li, Y.; Guan, Y.; Liu, Y.; Yin, J.; Zhao, X. Highly stable nanofluid based on polyhedral oligomeric silsesquioxane-decorated graphene oxide nanosheets and its enhanced electro-responsive behavior. *Nanotechnology* 2016, 27, 195702.

(16) Jiang, J.; Tian, Y.; Meng, Y. Structure Parameter of Electrorheological Fluids in Shear Flow. *Langmuir* **2011**, 27, 5814-5823.

(17) Sedlačík, M.; Mrlík, M.; Pavlínek, V.; Sáha, P.; Quadrat, O. Electrorheological properties of suspensions of hollow globular titanium oxide/polypyrrole particles. *Colloid Polym. Sci.* 2012, 290, 41-48.

(18) Zhang, W. L.; Liu, Y. D.; Choi, H. J. Graphene Oxide Coated Core–Shell Structured Polystyrene Microspheres and Their Electrorheological Characteristics Under Applied Electric Field. *J. Mater. Chem.* **2011**, 21, 6916–6921.

(19) McIntyre, E. C.; Oh, H. J.; Green, P. F. Electrorheological Phenomena in Polyhedral Silsesquioxane Cage Structure/PDMS Systems. *ACS Appl. Mater. Interfaces* **2010**, 2, 965-968.

(20) Song, Z.; Cheng, Y.; Wu, J.; Guo, J.; Xu, G. Influence of volume fraction on the yield behavior of giant electrorheological fluid. *Appl. Phys. Lett.* **2014**, 101, 101908.

(21) Wu, J.; Xu, G.; Cheng, Y.; Liu, F.; Guo, J.; Cui, P. The influence of high dielectric constant core on the activity of core–shell structure electrorheological fluid. *J. Colloid Interface Sci.* **2012**, 378, 36-43.

(22) Wu, J.; Liu, F.; Guo, J.; Cui, P.; Xu, G.; Cheng, Y. Preparation and electrorheological characteristics of uniform core/shell structural particles with different polar molecules shells. *Colloid Surf. A* **2012**, 410, 136-143.

(23) Cheng, Y.; Guo, J.; Liu, X.; Sun, A.; Xu, G.; Cui, P. Preparation of Uniform Titania Microspheres with Good Electrorheological Performance and Their Size Effect. *J. Mater. Chem.* **2011**, 21, 5051–5056.

(24) Wen, W.; Huang, X.; Yang, S.; Lu, K.; Sheng, P. The Giant Electrorheological Effect in Suspensions of Nanoparticles. *Nat. Mater.* **2003**, 2, 727–730.

(25) Huang, X.; Wen, W.; Yang, S.; Sheng, P. Mechanisms of the giant electrorheological effect. *Solid State Commun.* **2006**, 139, 581-588.

(26) Tan, P.; Tian, W. J.; Wu, X. F.; Huang, J. Y.; Zhou, L. W.; Huang, J. P. Saturated Orientational Polarization of Polar Molecules in Giant Electrorheological Fluids. *J. Phys. Chem. C* **2009**, 113, 9092-9097.

(27) Shen, R.; Wang, X.; Lu, Y.; Wang. D.; Sun, G.; Cao, Z.; Lu, K. Polar-Molecule-Dominated Electrorheological Fluids Featuring High Yield Stresses. *Adv. Mater.* **2009**, 21, 4631-4635.

(28) Raykar, V. S.; Sahoo, S. K.; Singh, A. K. Giant electrorheological effect in Fe_2O_3 nanofluids under low dc electric fields. *J. Appl. Phys.* **2010**, 108, 034306.

(29) Liu, Y. D.; Cheng, Y.; Xu, G.; Choi, H. J. Yield stress analysis of 1D calcium and titanium precipitate-based giant electrorheological fluids. *Colloid Polym. Sci.* **2013**, 291, 1267-1270.

(30) Yin, J. B.; Zhao, X. P. Giant electrorheological activity of high surface area mesoporous cerium-doped TiO_2 templated by block copolymer. *Chem. Phys. Lett.* **2004**, 398, 393-399.

(31) Hong, J.-Y.; Choi, M.; Kim, C.; Jang, J. Geometrical Study of Electrorheological Activity with Shape-Controlled Titania-Coated Silica Nanomaterials. *J. Colloid Interface Sci.* **2010**, 347, 177–182.

(32) Han, W. J.; Piao, S. H.; Choi, H. J. Synthesis and electrorheological characteristics of polyaniline@attapulgite nanoparticles via Pickering emulsion polymerization. *Materials Letters* **2017**, 204, 42-44.

(33) Yin, J.; Zhao, X. Titanate nano-whisker electrorheological fluid with high suspended stability and ER activity. *Nanotechnology* **2006**, 17, 192-196.

(34) Shin, K.; Kim, D.; Cho, J. C.; Lim, H. S.; Kim, J. W.; Suh, K. D. Monodisperse conducting colloidal dipoles with symmetric dimer structure for enhancing electrorheology properties. *J. Colloid Interface Sci.* **2012**, 374, 18-24.

(35) Orellana, C. S.; He, J.; Jaeger, H. M. Electrorheological response of dense strontium titanyl oxalate suspensions. *Soft Matter* **2011**, 7, 8023-8029.

(36) Xin, X.; Zhou, X.; Wu, J.; Yao, X.; Liu, Z. Scalable Synthesis of TiO_2/Graphene Nanostructured Composite with High-Rate Performance for Lithium Ion Batteries. *ACS Nano* **2012**, 6, 11035-11043.

(37) Cheng, Y.; Wu, K.; Liu, F.; Guo, J.; Liu, X.; Xu, G.; Cui, P. Facile Approach to Large-Scale Synthesis of 1D Calcium and Titanium Precipitate (CTP) with High Electrorheological Activity. *ACS Appl. Mater. Interfaces* **2010**, 2, 621-625.

(38) Song, Z.; Cheng, Y.; Guo, J.; Wu, J.; Xu, G.; Cui, P. Influence of thermal treatment on CTO wettability. *Colloid Surf. A* **2012**, 396, 305-309.

(39) Washburn, E. W. THE DYNAMICS OF CAPILLARY FLOK. *Phys. Rev.* **1921**, 17, 273-283.

(40) Wu, J.; Jin, T.; Liu, F.; Guo, J.; Cui, P.; Cheng, Y.; Xu, G. Preparation of rod-like calcium titanyl oxalate with enhanced electrorheological activity and their morphological effect. *J. Mater. Chem. C* **2014**, 2, 5629-5635.

(41) Gong, X.; Wu, J.; Huang, X.; Wen, W.; Sheng, P. Influence of liquid phase on nanoparticle-based giant electrorheological fluid. *Nanotechnology* **2008**, 19, 165602.

(42) Ikazaki, F.; Kawai, A.; Uchida, K.; Kawakami, T.; Edmura, K.; Sakurai, K.; Anzai, H.; Asako, Y. Mechanisms of electrorheology: the effect of the dielectric property. *J. Phys. D Appl. Phys.* **1998**, 31, 336-347.

(43) Hao, T.; Kawai, A.; Ikazaki, F. Mechanism of the Electrorheological Effect: Evidence from the Conductive, Dielectric, and Surface Characteristics of Water-Free Electrorheological Fluids. *Langmuir* **1998**, 14, 1256-1262.

(44) Whittle, M.; Bullough, W. A.; Peel, D. J.; Firoozian, R. Dependence of electrorheological response on conductivity and polarization time. *Phys. Rev. E* **1994**, 49, 5249-5259.

(45) Wang, Z.; Xuan, S.; Jiang, W.; Gong, X. The normal stress of an electrorheological fluid in compression mode. *RSC Adv.* **2017**, 7, 25855-25860.

(46) Wen, W.; Huang, X.; Sheng, P. Particle size scaling of the giant electrorheological effect. *Appl. Phys. Lett.* **2004**, 85, 299-301.

(47) Chen, S.; Huang, X.; van der Vegt, N. F. A.; Wen, W.; Sheng, P. Giant Electrorheological Effect: A Microscopic Mechanism. *Phys. Rev. Lett.* **2010**, 105, 046001.

(48) Ma, N.; Zhang, Z.; Dong, X.; Wang, Q.; Niu, C.; Han, B. Dynamic viscoelasticity and phenomenological model of electrorheological elastomers. *J. Appl. Polym. Sci.* **2017**, 134, 45407.

(49) Block, H.; Kelly, J. P.; Qin, A.; Watson, T. Materials and Mechanisms in Electrorheology. *Langmuir* **1990**, 6, 6-14.

(50) Kawai, A.; Ide, Y.; Inoue, A.; Ikazaki, F. Electrorheology of miscible blended liquid crystalline polymer: A dielectric property Approach. *J. Chem. Phys.* **1998**, 109, 4587-4591.

(51) Dong, Y.; Yin, J.; Yuan, J.; Zhao, X. Microwave-assisted synthesis and high-performance anhydrous electrorheological characteristic of monodisperse poly(ionic liquid) particles with different size of cation/anion parts. *Polymer* **2016**, 97, 408-417.

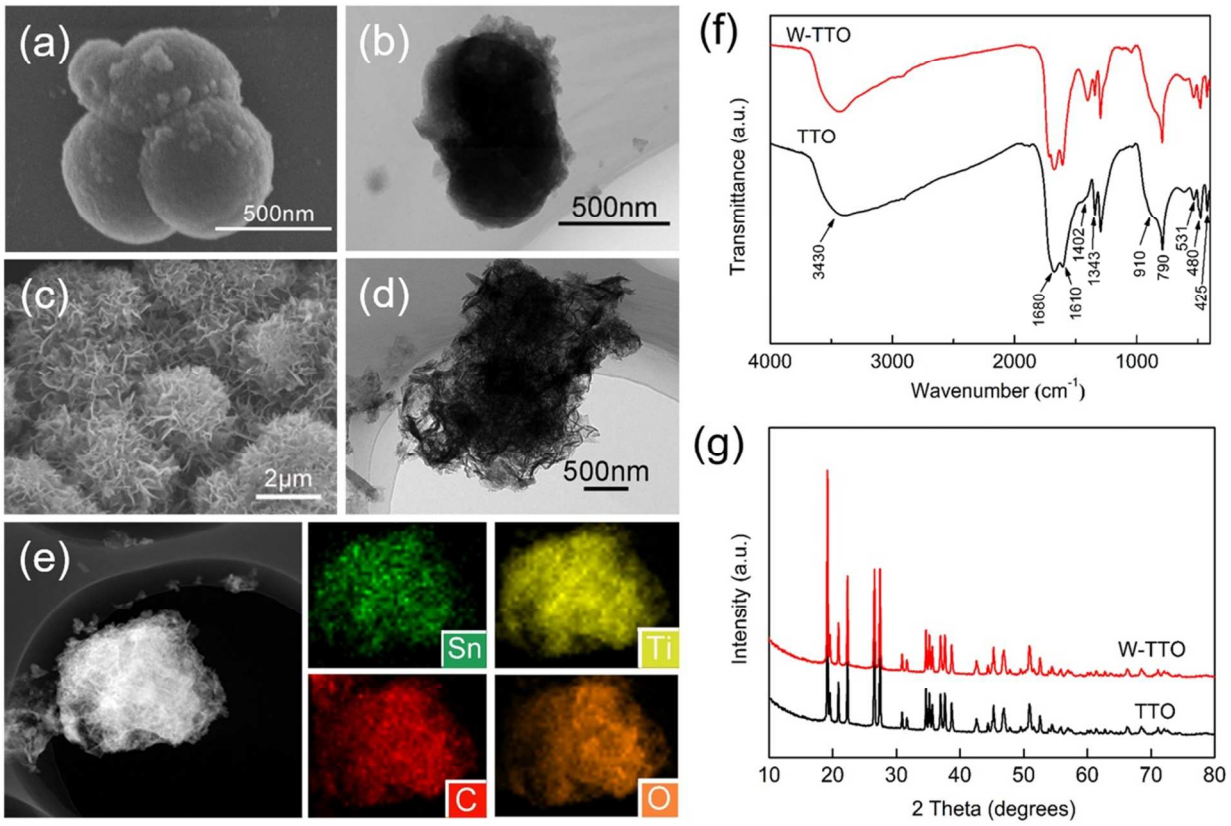

Figure 1. SEM and TEM images of TTO (a, b) and W-TTO (c, d); STEM elemental mapping images of W-TTO (e); FTIR spectra of the TTO and W-TTO particles (f); XRD patterns of the TTO and W-TTO (g).

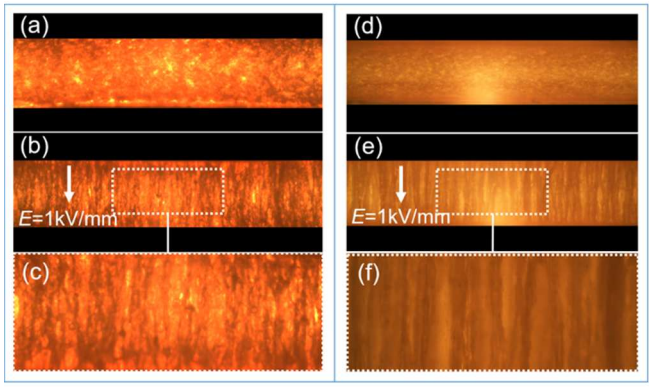

Figure 2. Optical microscopy images of TTO (a, b, c) and W-TTO (d, e, f) particles in the presence of electric field (dashed line box is the enlarged view).

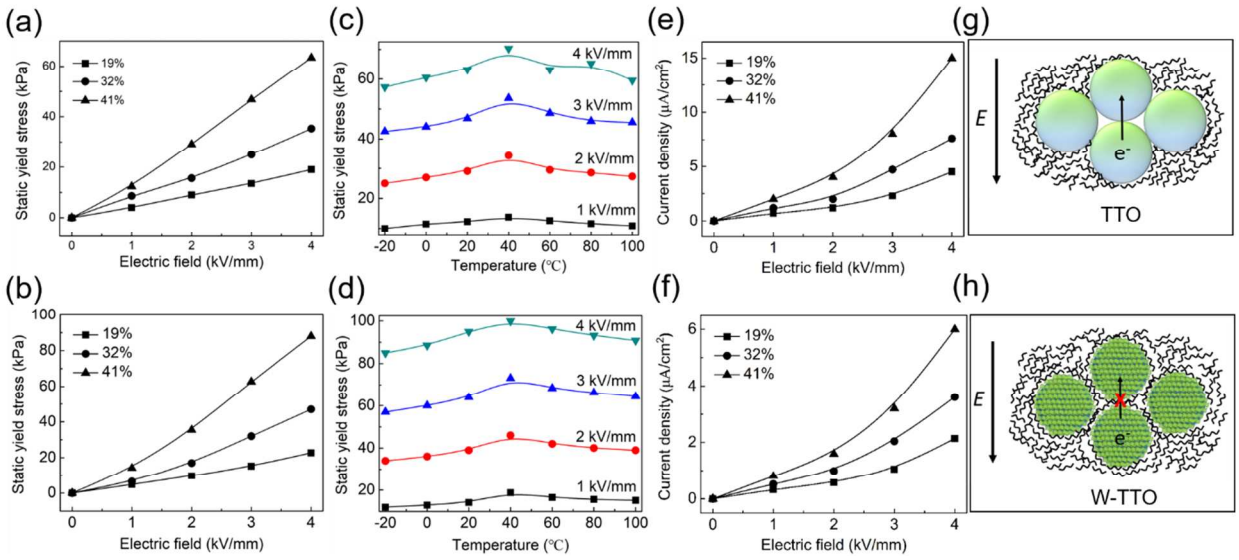

Figure 3. Static yield stress of the TTO (a) and W-TTO (b) ER fluids as a function of applied electric field; static yield stresses of the TTO (c) and W-TTO (d) ER fluids under different temperatures; leakage current density of the TTO (e) and W-TTO (f) ER fluids as a function of applied electric field; schematic illustration of TTO (g) and W-TTO (h) dispersion in silicone oil under electric field.

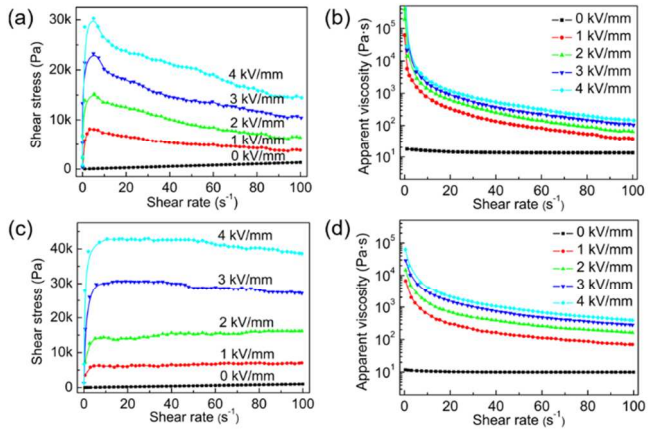

Figure 4. Shear stress and apparent viscosity of TTO (a, b) and W-TTO (c, d) ER fluids at volume fraction 32% as a function of shear rate under various electric fields.

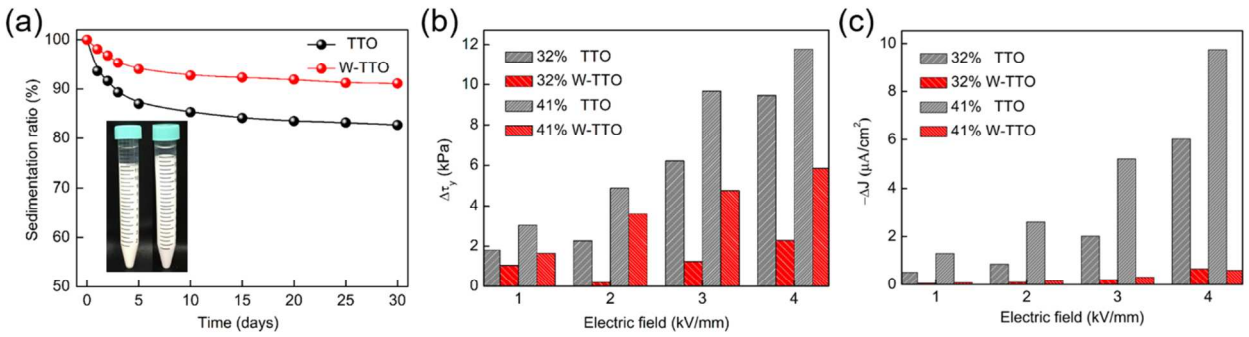

Figure 5. Time stability of the TTO and W-TTO ER fluids: Sedimentation ratio as a function of ageing time (particle concentration is 32%) (a); the difference for static yield stress $\Delta\tau_y$ (b) and leakage current density ΔJ (c) of TTO and W-TTO as a function of applied electric field after sedimentation for 30 days (where τ_y and J is static yield stress and leakage current density respectively).

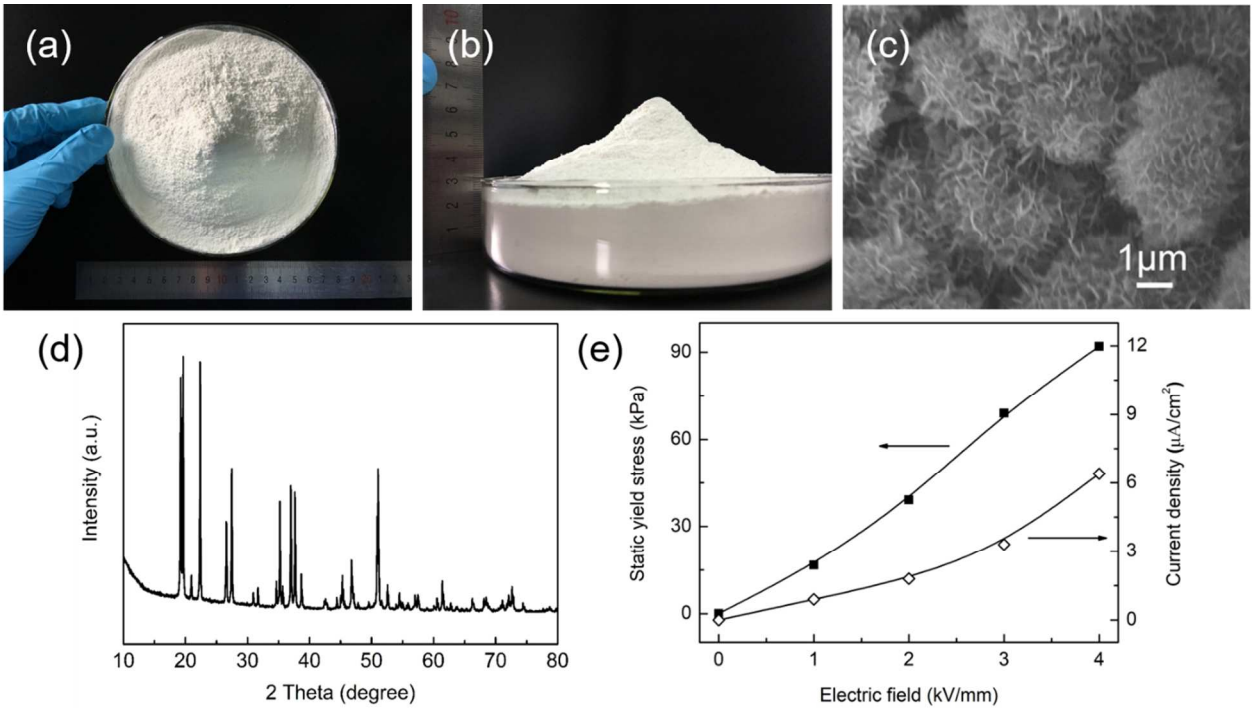

Figure 6. Photographs (a, b); SEM image (c); XRD pattern (d); static yield stress and leakage current density under various electric fields (e) of W-TTO particles prepared at a large scale.

Table 1. Dielectric characteristics of the TTO and W-TTO ER fluids.

Sample	ε'_{50}	$\varepsilon'_{10\text{^}6}$	$\Delta\varepsilon'$ [a)]	λ (s) [b)]
TTO	15.09	6.36	8.73	2.36×10^{-4}
W-TTO	25.41	6.57	18.84	1.06×10^{-4}

[a)] The $\Delta\varepsilon'$ of particles calculated by equation $\Delta\varepsilon' = \varepsilon'_{50} - \varepsilon'_{10\text{^}6}$; [b)] The λ(s) of particles calculated by equation $\lambda(s) = 1/2\pi f_{max}$ approximately (where f_{max} is the frequency corresponding to the maximum of dielectric loss factor).

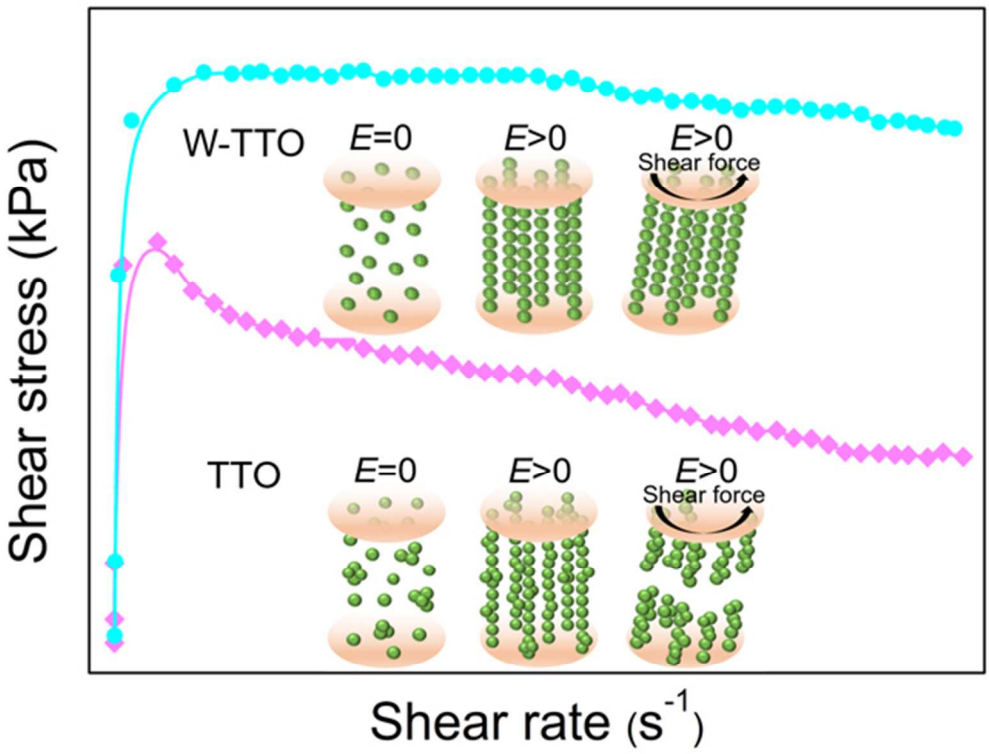

Table of Contents

55x41mm (300 x 300 DPI)